molecules

MDPI

Article

Continuous Electrochemical Reduction of CO_2 to Formate: Comparative Study of the Influence of the Electrode Configuration with Sn and Bi-Based Electrocatalysts

Guillermo Díaz-Sainz *, Manuel Alvarez-Guerra and Angel Irabien

Chemical and Biomolecular Engineering Department, University of Cantabria, ETSIIT, Avda. Los Castros s/n, 39005 Santander, Spain; manuel.alvarezg@unican.es (M.A.-G.); angel.irabien@unican.es (A.I.)

* Correspondence: diazsg@unican.es

Academic Editors: José Solla Gullón and Paramaconi Rodriguez

Received: 27 August 2020; Accepted: 25 September 2020; Published: 28 September 2020

Abstract: Climate change has become one of the most important challenges in the 21st century, and the electroreduction of CO_2 to value-added products has gained increasing importance in recent years. In this context, formic acid or formate are interesting products because they could be used as raw materials in several industries as well as promising fuels in fuel cells. Despite the great number of studies published in the field of the electrocatalytic reduction of CO_2 to formic acid/formate working with electrocatalysts of different nature and electrode configurations, few of them are focused on the comparison of different electrocatalyst materials and electrode configurations. Therefore, this work aims at presenting a rigorous and comprehensive comparative assessment of different experimental data previously published after many years of research in different working electrode configurations and electrocatalysts in a continuous mode with a single pass of the inputs through the reactor. Thus, the behavior of the CO_2 electroreduction to formate is compared operating with Sn and Bi-based materials under Gas Diffusion Electrodes (GDEs) and Catalyst Coated Membrane Electrodes (CCMEs) configurations. Considering the same electrocatalyst, the use of CCMEs improves the performance in terms of formate concentration and energy consumption. Nevertheless, higher formate rates can be achieved with GDEs because they allow operation at higher current densities of up to 300 $mA{\cdot}cm^{-2}$. Bi-based-GDEs outperformed Sn-GDEs in all the figures of merit considered. The comparison also highlights that in CCME configuration, the employ of Bi-based-electrodes enhanced the behavior of the process, increasing the formate concentration by 35% and the Faradaic efficiency by 11%.

Keywords: CO_2 valorization; electroreduction; formate; Sn-based materials; bi-based materials; gas diffusion electrodes (GDEs); catalyst coated membrane electrodes (CCMEs); comparative analysis

1. Introduction

Carbon dioxide (CO_2) emissions to the atmosphere have gradually increased since the middle of the twentieth century from 326 ppm in 1971 to approximately 417 ppm in 2020 [1]. According to the Sustainable Development Goals (SDGs) established by the United Nations and particularly, to SDG Number 13 defined as Climate Action, CO_2 is the most important human-emitted greenhouse gas in the atmosphere. Therefore, shrinking the CO_2 emissions should be considered as one of the most important priorities in the current century to mitigate climate change [2].

Different strategies can be considered to reduce CO_2 emissions to the atmosphere, such as improving the energy efficiency or developing renewable energy sources and related technologies [3,4]. In this sense, Carbon Capture, Storage and Utilization (CCSU) [5–9] have been suggested as promising

approaches for mitigating climate change. In particular, the possibility of converting captured CO_2 into fuels and useful industrial chemicals has been especially pointed out [10,11].

Indeed, CO_2 can be transformed to value-added chemical products by several routes, such as thermochemical processes or mineralization [12], biological transformation [13], electrochemical [14] or photochemical/photoelectrochemical conversion [15]. Among these approaches, the electrochemical reduction of CO_2 toward chemicals with value added has been suggested as an excellent way to store energy from renewable sources in the form of chemical products [16,17].

In this respect, different valued-added products [18,19] can be obtained by CO_2 electrocatalytic reduction such as carbon monoxide (CO) [20,21], formic acid (HCOOH) or formate ($HCOO^-$) [22,23] or methanol (CH_3OH), ethylene (C_2H_4), and methane (CH_4) [24–28].

Among these products, HCOOH or $HCOO^-$, depending on pH, are used as raw material in several industries (leather tanning, animal feed, steel pickling, or pharmaceutical) [29]. Furthermore, this product has been recommended as an interesting fuel for low-temperature fuel cells [30,31], as well as a promising hydrogen carrier [32,33]. According to the literature [22,34,35], electrocatalysts of different nature, different electrode configurations, and different electrochemical reactors have been used for studying the electrocatalytic reduction of CO_2 to HCOOH/$HCOO^-$. On the one hand, copper (Cu) [36], cobalt (Co) [37], molybdenum (Mo) [38], lead (Pb) [39–41], indium (In) [42–44], palladium (Pd) [45,46], and especially tin (Sn) [47–54] and bismuth (Bi) [55–62] are the most common catalysts investigated for the selective electrochemical reduction of CO_2 to HCOOH/$HCOO^-$. On the other hand, the electrocatalyst can be used in different electrode configurations, such as in the form of a metal plate, a Gas Diffusion Electrode (GDE), or a Catalyst Coated Membrane Electrode (CCME), operating with different electrochemical reactor configurations and operating conditions.

Moreover, an important problem in CO_2 electroreduction is that many different variables may have an influence on the results, which makes it very difficult to compare the results of studies carried out in different experimental conditions. Although there is a great number of studies that focused on the CO_2 electroreduction to obtain HCOOH/$HCOO^-$ using electrocatalysts of diverse nature or cathode configuration, few of them focused on thorough comparisons of the performance of the electrochemical process operating with different catalyst materials and electrode configurations with the same experimental setup and operating conditions [63–65]. In this context, this work aims to rigorously compare the behavior of the CO_2 electroreduction to obtain $HCOO^-$ using the same experimental setup but employing electrocatalysts of a different nature, (i) Sn carbon-supported nanoparticles (Sn/C NPs) and (ii) Bi carbon-supported nanoparticles (Bi/C NPs), and under different electrode configurations: (i) GDEs and (ii) CCMEs. The experimental data needed to achieve the aim of manuscript have been previously published after many years of research of our group. A comparative assessment is performed in terms of different relevant figures of merit, including $HCOO^-$ concentration, $HCOO^-$ rate, Faradaic efficiency for $HCOO^-$ (FE), and consumption of energy per kmol of $HCOO^-$.

2. Comparative Study of the Electrode Configurations: GDE–CCME

This section will compare the performance of GDE and CCME electrode configuration for the electroreduction of CO_2 to $HCOO^-$, employing the same experimental setup and the same electrocatalyst. The comparison will be made first considering the same Sn-based catalyst and then using the same Bi-based catalyst.

2.1. Sn-Based Electrodes

The results of different experiments carried out with the same catalyst (Sn NPs) using different working electrode configurations—GDEs (Sn/C-GDEs) and CCMEs (Sn/C-CCMEs)—are reported and discussed in references [66,67], respectively. A summary of the main results of the performance with both configurations is summarized in Table 1. Although the operating conditions were the same, depositing directly the catalytic material over the membrane (Sn/C-CCME) instead of depositing the catalyst over a carbonaceous support (Sn/C-GDE) improved the performance of the electrochemical process,

as shown in Table 1. Noteworthy results in terms of $HCOO^-$ concentration and energy consumption per kmol of $HCOO^-$ using the Sn-based catalyst can be obtained using Sn/C-CCME as a cathode in the electrochemical reactor, with values of 19.2 $g{\cdot}L^{-1}$ and 244 $kWh{\cdot}kmol^{-1}$, respectively, which represent noticeably better results than those with the Sn/C-GDE configuration. This improvement can be in part attributed to the better behavior of the electrochemical reactor using a solid polymer electrolyte (with the Sn/C-CCME configuration) instead of a liquid electrolyte (with the Sn/C-GDE configuration). This may be attributed to the fact that the humidified CO_2 gas input stream enhances the delivery of gaseous CO_2 to the working electrode surface, and therefore, the solubility limitation of CO_2 in the electrolyte.

Table 1. Figures of merit (current density, flow in the cathode side, $HCOO^-$ concentration, $HCOO^-$ rate, Faradaic efficiency (FE) for $HCOO^-$ and energy consumption per kmol of $HCOO^-$) for the electrocatalytic reduction of CO_2 to $HCOO^-$ employing different Sn-based electrodes (Sn/C-GDEs and Sn/C-CCMEs). Data taken from references [66,67].

Figures of Merit	Configuration				
	Sn/C-GDEs [66]				Sn/C-CCMEs [67]
Flow in the cathode side ($mL{\cdot}min^{-1}$)	5.7	5.7	5.7	0.7	~0.008 (0.5 $g{\cdot}h^{-1}$)
Current density ($mA{\cdot}cm^{-2}$)	90	150	200	200	45
Absolute cell potential (V)	3.1	3.7	4.0	4.3	2.2
$HCOO^-$ concentration ($g{\cdot}L^{-1}$)	1.5	2.5	2.7	16.9	19.2
$HCOO^-$ rate ($mmol{\cdot}m^{-2}{\cdot}s^{-1}$)	3.23	5.45	5.61	4.38	1.15
FE for $HCOO^-$ (%)	69.4	70	54.1	42.3	49.4
Energy consumption ($kWh{\cdot}kmol^{-1}$)	239	282	396	513	244

Despite the improvement in the $HCOO^-$ concentration and the energy consumption per kmol of $HCOO^-$, the $HCOO^-$ rate and the FE for $HCOO^-$ did not show a substantial enhancement. As can be seen in Table 1, the FE for $HCOO^-$ was very similar in both configurations (42.3 and 49.4%), and the $HCOO^-$ rate obtained using the Sn/C-CCME configuration decreased from 4.38 to 1.15 $mmol{\cdot}m^{-2}{\cdot}s^{-1}$ because of the low values of current density supplied to the electrochemical reactor using the Sn/C-CCME cathode (45 $mA{\cdot}cm^{-2}$) configuration with respect to Sn/C-GDE configuration (90, 150, and 200 $mA{\cdot}cm^{-2}$). In this sense, the current density employed in Sn/C-CCME was fixed to that value, since an increase in this variable results in higher cell potentials with respect to the use of Sn/C-GDE at the same operating conditions.

Thus, it can be concluded that an Sn/C-GDE configuration is more suitable for operating at higher current densities, and therefore achieving higher rates of CO_2 reduction and formation of product, but the process results are more energetically favorable under an Sn/C-CCME configuration.

2.2. Bi-Based Electrodes

In Table 2, the comparison between the GDE configuration (Bi/C-GDE) [68] and the CCME configuration (Bi/C-CCME) [69], employing the same Bi/C NPs as electrocatalyst, is carried out, in terms of $HCOO^-$ concentration, $HCOO^-$ rate, FE for $HCOO^-$, and the energy consumption per kmol of $HCOO^-$.

Table 2. Figures of merit (current density, $HCOO^-$ concentration, $HCOO^-$ rate, FE for $HCOO^-$, and energy consumption per kmol of $HCOO^-$) for the electrocatalytic reduction of CO_2 to $HCOO^-$ employing different Bi-based electrodes (GDEs and CCMEs). Data taken from references [68,69].

Figures of Merit	Configuration					
	Bi/C-GDEs [68]					Bi/C-CCMEs [69]
Flow in the cathode side ($mL \cdot min^{-1}$)	5.7	5.7	5.7	5.7	0.7	~0.008 (0.5 $g \cdot h^{-1}$)
Current density ($mA \cdot cm^{-2}$)	90	150	200	300	200	45
Absolute cell potential (V)	3.1	3.7	4.2	5.4	4.5	2.7
$HCOO^-$ concentration ($g \cdot L^{-1}$)	2.0	3.06	3.9	5.2	18.0	25.9
$HCOO^-$ rate ($mmol \cdot m^{-2} \cdot s^{-1}$)	4.31	6.46	8.33	10.97	4.67	1.28
FE for $HCOO^-$ (%)	92.4	83.1	80.4	70.6	45.1	54.8
Energy consumption ($kWh \cdot kmol^{-1}$)	177	240	277	410	535	266

It is noteworthy that Bi/C-GDEs were able to operate with a high current density up to 300 $mA \cdot cm^{-2}$, obtaining an $HCOO^-$ concentration of 5.2 $g \cdot L^{-1}$ with an FE for $HCOO^-$ of 70.6%, an $HCOO^-$ rate of 10.97 $mmol \cdot m^{-2} \cdot s^{-1}$, and an energy consumption per kmol of $HCOO^-$ of 410 $kWh \cdot kmol^{-1}$ of $HCOO^-$. Nevertheless, the possibility of obtaining higher $HCOO^-$ concentration (18.0 $g \cdot L^{-1}$) with Bi/C-GDEs was by means of lowering the catholyte flow and at the expense of a decrease in both FE for $HCOO^-$ (45.1%) and $HCOO^-$ rate (4.67 $mmol \cdot m^{-2} \cdot s^{-1}$). As illustrated in Table 2, working with a Bi/C-CCME configuration, promising results can be achieved in terms of $HCOO^-$ concentration, FE for $HCOO^-$, and energy consumption per kmol of $HCOO^-$. The best result using a Bi/C-CCME configuration allowed obtaining an $HCOO^-$ concentration approximately 44% higher with respect to the highest $HCOO^-$ concentration obtained using Bi/C-GDE, and simultaneously, the FE for to $HCOO^-$ is approximately 21.5% higher with an important saving in the energy consumption per kmol of $HCOO^-$ of around 50%. Similarly, as was found for Sn-based electrodes, the $HCOO^-$ rate decreased using a Bi/C-CCMEs configuration with respect to the Bi/C-GDE configuration because of the lower current densities supplied to the electrochemical filter press by potentiostat–galvanostat.

Finally, as can be concluded from the analysis of the results in Table 2, the Bi/C-CCME configuration improves the performance of the electrochemical conversion of CO_2 to $HCOO^-$ in terms of $HCOO^-$ concentration, FE for $HCOO^-$, and the energy consumption per kmol of $HCOO^-$. However, the $HCOO^-$ rate did not show an important improvement for the electrocatalytic reduction of CO_2 to $HCOO^-$ because the CCME configuration did not allow operating with high current densities values.

3. Comparative Study of the Catalyst Nature

This section is focused on the comparison of the performance of the CO_2 electroreduction to obtain $HCOO^-$ employing two electrocatalysts of different nature: Sn carbon-supported nanoparticles (Sn/C NPs) and Bi carbon-supported nanoparticles (Bi/C NPs), considering the same experimental setup and the same electrode configuration. The comparison of the two catalysts will be made first using a GDE configuration and then employing a CCME configuration.

3.1. Sn vs. Bi in GDE Configuration

A comparative study of the behavior of Sn/C NPs and Bi/C NPs in the form of a GDE is performed. For a clearer visualization, the results obtained using the GDE configurations with Sn/C NPs and Bi/C NPs are summarized in Figures 1 and 2.

As explained in Section 2, the current density and the catholyte flow per geometric area are considered the most influential variables in the performance of the process for the electrochemical conversion of CO_2 to $HCOO^-$ with GDEs The influence of current density in FE for $HCOO^-$ (Figure 1a) and the $HCOO^-$ rate (Figure 1b) with both electrocatalytic materials can be clearly studied in Figure 1. The current density ranged between 90 and 300 mA·cm^{-2} operating with the same catholyte flow (5.7 mL·min^{-1}) to allow a fair comparison. Nevertheless, it was not feasible to supply current densities higher than 200 mA·cm^{-2} using Sn/C-GDEs because of the high cell potential obtained operating with this current density (>4 V). Despite the decrease in the FE for $HCOO^-$, from 69 to 55% (with Sn/C-GDEs as working electrode) and from 92 to 80% (with Bi/C-GDEs as working electrode), when the current increased from 90 to 200 mA·cm^{-2}, an increase in the $HCOO^-$ rate was observed. Moreover, it is important to point out that a noteworthy result in terms of FE for $HCOO^-$, of approximately 70%, was achieved using Bi/C-GDEs supplied with a current density of 300 mA·cm^{-2}.

As illustrated in Figure 1b, on the one hand, the $HCOO^-$ rate using Sn/C-GDEs increased approximately 70% (from 3.23 to 5.61 mmol·m^{-2}·s^{-1}) when the current density increased from 90 to 200 mA·cm^{-2}. In contrast, $HCOO^-$ rates up to 8.33 mmol·m^{-2}·s^{-1} were obtained using Bi/C-GDEs, which was approximately 50% higher than those with Sn/C-GDE under the same operating conditions and with a current density of 200 mA·cm^{-2}. Nevertheless, the highest $HCOO^-$ rate was obtained with a current density of 300 mA·cm^{-2} (with Bi/C-GDEs as working electrode), achieving an excellent value of 10.97 mmol·m^{-2}·s^{-1}.

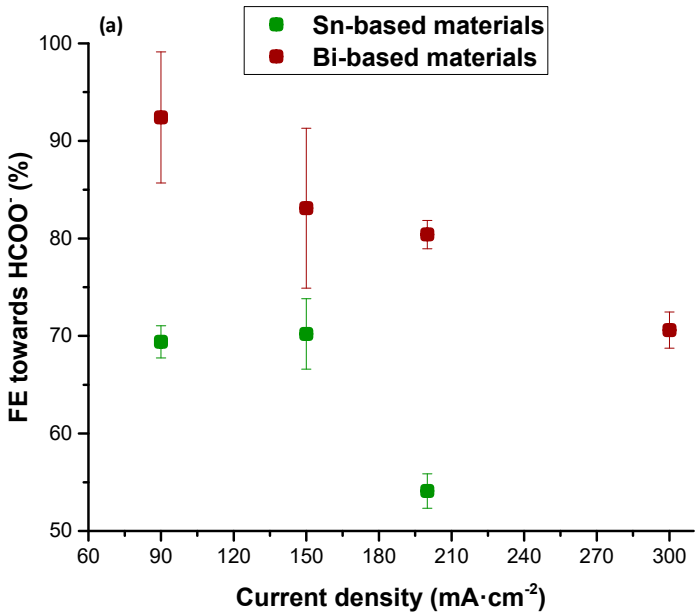

Figure 1. *Cont.*

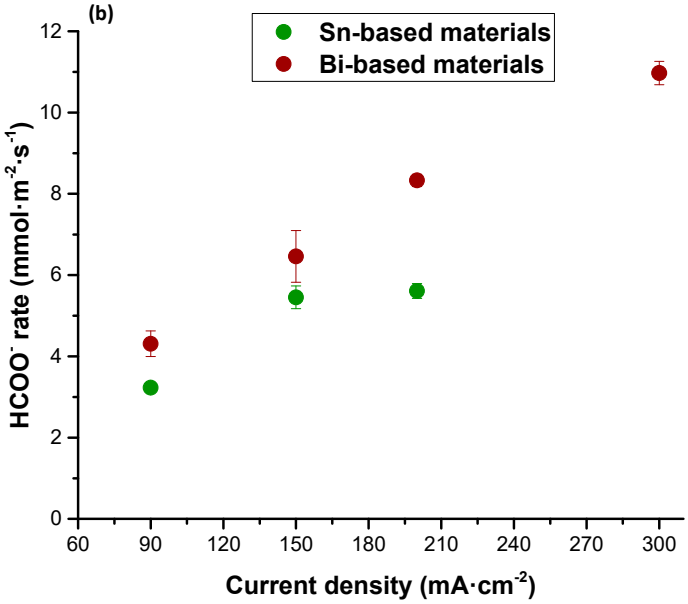

Figure 1. Influence of current density on (**a**) Faradaic Efficiency for $HCOO^-$ (%) and (**b**) $HCOO^-$ rate ($mmol \cdot m^{-2} \cdot s^{-1}$) in the current density range of 90–300 $mA \cdot cm^{-2}$ operating with an electrolyte flow = 5.7 $mL \cdot min^{-1}$. Sn/C-GDEs and Bi/C-GDEs are indicated in green and red, respectively. Data taken from references [66,68]. Sn-C: Sn carbon-supported nanoparticles; Bi/C: Sn carbon-supported nanoparticles.

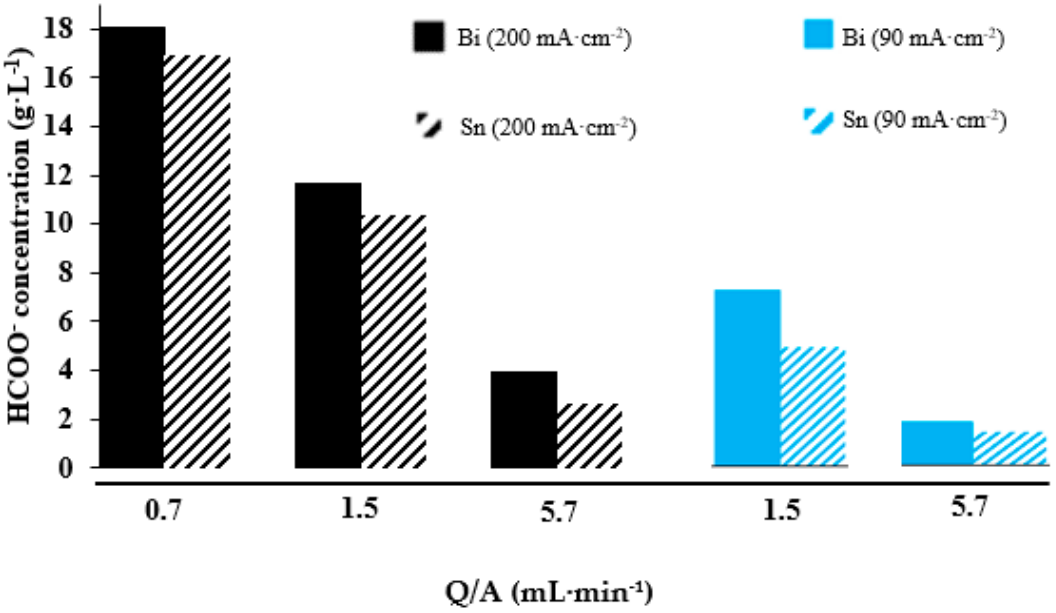

Figure 2. Influence of electrolyte flow on the $HCOO^-$ concentration ($g \cdot L^{-1}$) in the electrolyte flow range of 0.7–5.7 $mL \cdot min^{-1}$ applied at different current densities: 90 and 200 $mA \cdot cm^{-2}$ and with different electrocatalyst material (Sn/C NPs and Bi/C NPs). Data taken from references [66,68].

A summary of the results in terms of $HCOO^-$ concentration obtained at different current densities and catholyte flows is represented in Figure 2. On the one hand, operating at a certain same current density (90 or 200 $mA \cdot cm^{-2}$), a higher $HCOO^-$ concentration collected in the output stream of the electrochemical filter press cell is obtained if the catholyte flow is lowered from 5.7 to 0.7 $mL \cdot min^{-1} \cdot cm^{-2}$. As happened with the FE and the $HCOO^-$ rate, the performance of the electrochemical cell in terms of $HCOO^-$ concentration is better working with Bi/C-GDEs than with Sn/C-GDEs. The highest $HCOO^-$ concentration obtained was 18.0 $g \cdot L^{-1}$, which was 7% higher than operating with the same value of current density and catholyte flow in Sn/C-GDEs (Figure 2). However, working with a current density

= 200 mA·cm^{-2}, the highest difference between the Bi/C-GDEs and the Sn/C-GDEs was operating with a catholyte flow = 5.7 mL·min^{-1}, obtaining an $HCOO^-$ concentration of 3.95 g·L^{-1} (using Bi/C-GDE as cathode), which was 50% higher with respect to the value of $HCOO^-$ concentration using Sn/C-GDE.

In addition, the comparison of Bi and Sn-based GDEs in terms of energy consumption per kmol of $HCOO^-$ is summarized in Table 3. Bi-based electrocatalysts in the form of GDEs resulted in needing less energy consumption per kmol of $HCOO^-$ at different current densities and catholyte flows compared with Sn/C GDEs.

Table 3. Energy consumption per kmol of $HCOO^-$ for the electrocatalytic reduction of CO_2 to $HCOO^-$ working with Sn/C-GDEs and Bi/C-GDEs at different operating conditions (current density and catholyte flow). Data taken from references [66,68].

Operating Condition		Energy Consumption (kWh·kmol^{-1} of $HCOO^-$)	
Current Density (mA·cm^{-2})	**Catholyte Flow (mL·min^{-1})**	**Sn/C-GDEs [66]**	**Bi/C-GDEs [68]**
90	5.7	239	177
150		282	240
200		396	277
90	1.5	267	186
200		395	364
	0.7	544	535

After the analysis of these results, it can be concluded that the use of GDEs with Bi/C NPs gives better results for the electrocatalytic reduction of CO_2 to $HCOO^-$ in terms of all figures of merit studied (FE for $HCOO^-$, $HCOO^-$ rate, $HCOO^-$ concentration and energy consumption per kmol of $HCOO^-$). Moreover, it should be highlighted that Bi/C-GDEs allow operating with remarkable values of current density (300 mA·cm^{-2}). In the next section, a similar comparison was carried out between Bi/C NPs and Sn/C NPs in the form of CCMEs.

3.2. Sn vs. Bi in CCME Configuration

As previously discussed in Section 2, the key variables studied in the CCMEs configuration are the temperature and the water flow in the input CO_2 stream [67,69]. In order to compare the performance of Sn/C-CCMEs and Bi/C-CCMEs, all the experiments considered for the study in this section were carried out operating with a catalyst load = 0.75 mg·cm^{-2} and a current density = 45 mA·cm^{-2}.

First, a comparative of the performance of Sn/C-CCMEs and Bi/C-CCMEs at different temperatures is carried out in terms of Faradaic efficiency for $HCOO^-$ (Figure 3a), $HCOO^-$ rate (Figure 3b), energy consumption per kmol of $HCOO^-$ (Figure 3c), and $HCOO^-$ concentration (Figure 3d). The range of temperature studied in both configurations was between 20 and 50 °C. Using either Bi or Sn as electrocatalyst, when the temperature was increased from 20 to 50 °C, all the figures of merit analyzed in this work got worse due to the promotion of the hydrogen evolution reaction. The best results were obtained using Bi-based electrodes operating at ambient condition of temperature, whereas when the temperature was increased to 50 °C, the best performance of the electrochemical process was with the use of Sn/C NPs instead of Bi/C NPs.

Supplying the CO_2 stream to the electrochemical reactor with Bi-based CCMEs at a temperature = 20 °C, the FE for $HCOO^-$, the $HCOO^-$ rate, the energy consumption per kmol of $HCOO^-$, and the $HCOO^-$ concentration obtained were 47.2%, 1.10 mmol·m^{-2}·s^{-1}, 312.1 kWh·kmol^{-1}, and 22.3 g·L^{-1}, respectively. Nevertheless, at the same conditions and using Sn/C-CCMEs, the figures of merit obtained were 47.3%, 1.10 mmol·m^{-2}·s^{-1}, 226.6 kWh·kmol^{-1}, and 18.4 g·L^{-1}, respectively. Therefore, although the FE and the $HCOO^-$ rate were very similar, the employ of Bi as electrocatalyst gives the best result in terms of $HCOO^-$ concentration (21% higher with Bi), and the use of Sn gives better

results in term of energy consumption per kmol of $HCOO^-$ (27% lower consumption than with Bi). It is interesting to reiterate that raising the temperature from 20 to 50 °C resulted in worse results in terms of all the figures of merit, as illustrated in Figure 3.

The influence of the water flow in the CO_2 stream was compared operating at ambient condition of temperature (20 °C) in the CO_2 input stream to the electrochemical reactor, as summarized graphically in Figure 4. The range of the water flow in the CO_2 stream studied using both catalyst materials ranged from 0.15 to 1 $g{\cdot}h^{-1}$. It can be seen in Figure 4a,b that the results of FE and rate obtained using Sn-based electrodes and Bi-based electrodes were very similar in the range of water flow studied. However, the performance of the electrochemical filter press cell was optimized with a water flow in the CO_2 stream = 0.5 $g{\cdot}h^{-1}$. On the one hand, using Bi in the form of CCMEs, a FE, a $HCOO^-$ rate, an energy consumption, and a $HCOO^-$ concentration of 54.8%, 1.28 $mmol{\cdot}m^{-2}{\cdot}s^{-1}$, 265.8 $kWh{\cdot}kmol^{-1}$, and 25.9 $g{\cdot}L^{-1}$, were obtained, respectively. Nevertheless, using Sn/C-CCMEs with the same operating conditions, the $HCOO^-$ concentration lowered 35 points in percentage to 19.2 $g{\cdot}L^{-1}$, keeping similar values in terms of FE, $HCOO^-$ rate, and energy consumption (49.4%, 1.15 $mmol{\cdot}m^{-2}{\cdot}s^{-1}$, and 244 $kWh{\cdot}kmol^{-1}$, respectively).

In both kinds of electrodes (Sn-based CCMEs and Bi-based CCMEs), raising the water flow in the CO_2 input stream from 0.5 to 1 $g{\cdot}h^{-1}$, the behavior of the electrochemical process to give $HCOO^-$ in terms of all figures of merit analyzed got worse. On the one hand, the FE and the $HCOO^-$ rate (Figure 4a,b) lowered from 54.8% to 47.8% and from 1.28 to 1.11 $mmol{\cdot}m^{-2}{\cdot}s^{-1}$, respectively, with the use of Bi-based electrodes, and at the same conditions under the Sn-CCME configuration, the FE decreased from 49.4% to 46.3% and the $HCOO^-$ rate decreased from 1.15 to 1.08 $mmol{\cdot}m^{-2}{\cdot}s^{-1}$, respectively. On the other hand, as illustrated in Figure 4c,d, the $HCOO^-$ concentration decreased from 25.9 to 22.6 $g{\cdot}L^{-1}$ and from 19.2 to 17.5 $g{\cdot}L^{-1}$, whereas the energy consumption per kmol of $HCOO^-$ increased to 319.9 and 249 $kWh{\cdot}kmol^{-1}$ using Bi-based and Sn-based electrodes, respectively.

Furthermore, the results show that the use of Bi-based materials in the form of CCMEs improves the performance of the electrochemical process for the electrocatalytic reduction of CO_2 to $HCOO^-$ in terms of FE for $HCOO^-$, $HCOO^-$ rate, and $HCOO^-$ concentration. However, the employ of Sn/C NPs in the form of CCMEs working at the same operating conditions allows obtaining $HCOO^-$ with less energy consumption per kmol of $HCOO^-$.

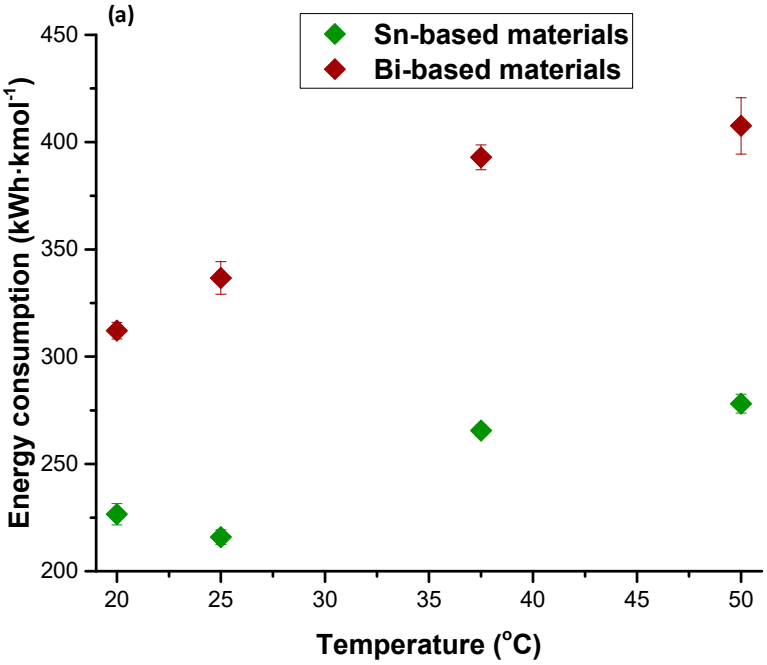

Figure 3. *Cont.*

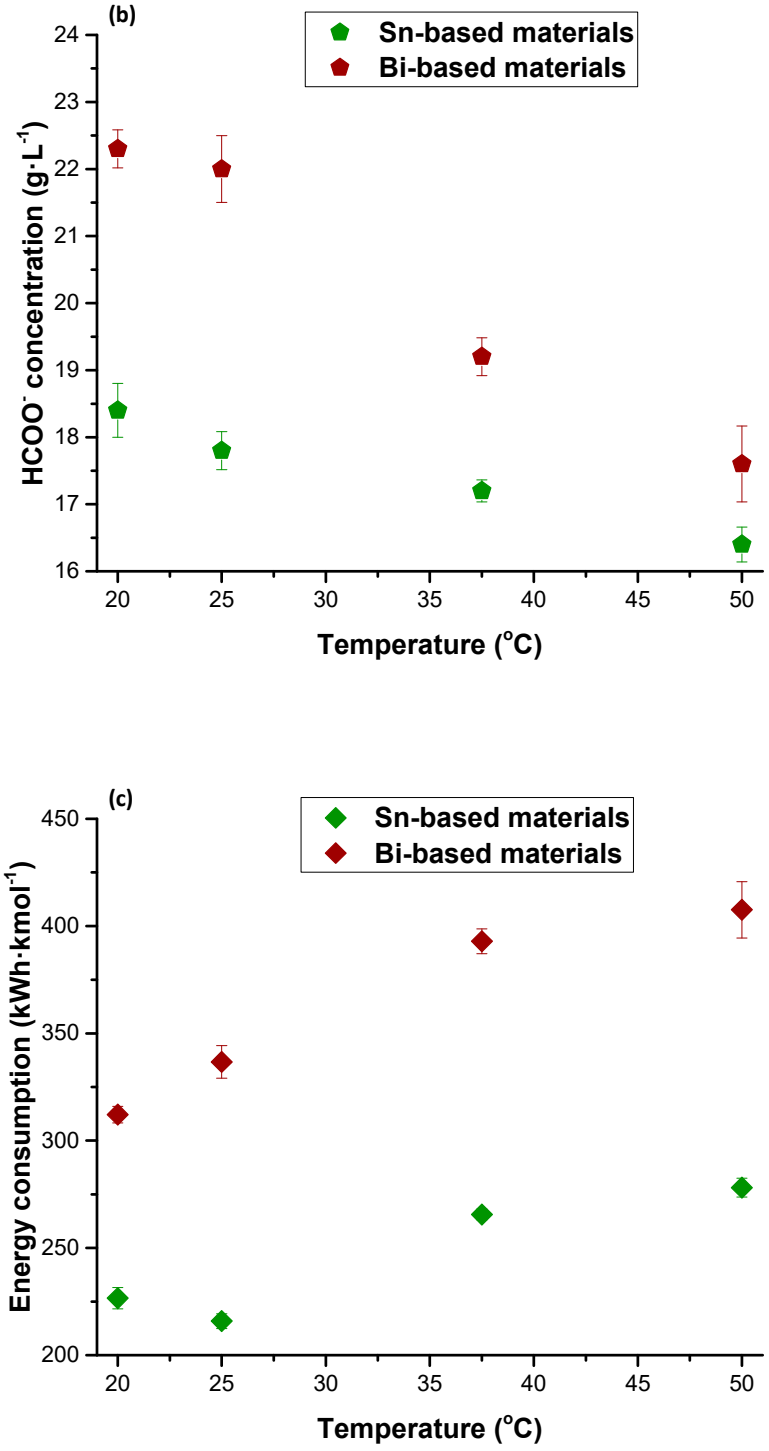

Figure 3. *Cont.*

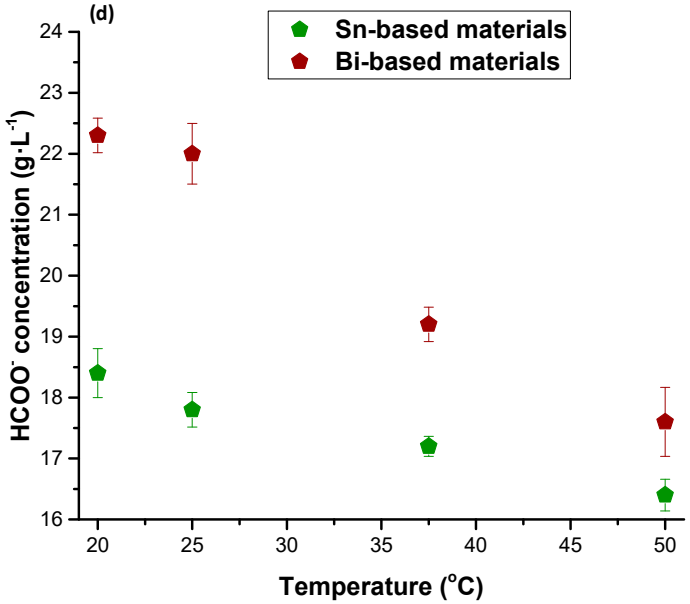

Figure 3. Influence of temperature on (**a**) Faradaic Efficiency for $HCOO^-$ (%), (**b**) $HCOO^-$ rate ($mmol \cdot m^{-2} \cdot s^{-1}$), (**c**) energy consumption per kmol of $HCOO^-$ ($kWh \cdot kmol^{-1}$), and (**d**) $HCOO^-$ concentration ($g \cdot L^{-1}$) in the temperature range of 20–50 °C applied at a constant current density = 45 $mA \cdot cm^{-2}$, a catalyst loading = 0.75 $mg \cdot cm^{-2}$, and a relative humidity = 100%. Sn/C-CCMEs and Bi/C-CCMEs are indicated in green and red, respectively. Data taken from references [67,69].

Finally, further research is still required to overcome current limitations and develop processes with performances that simultaneously optimize all the figures of merit analyzed in this study. In this regard, research efforts should focus on the development of new filter press configurations [70,71] such as the use of a three-compartment electrochemical reactor, bipolar membranes [72], or working electrode configurations [73] to enhance the mass transfer of the reagents and products in the counter and working electrode, and simultaneously address the synthesis of innovative electrocatalysts for both cathode [74] and anode [75] to reduce the energy consumption in both compartments of the electrochemical reactor.

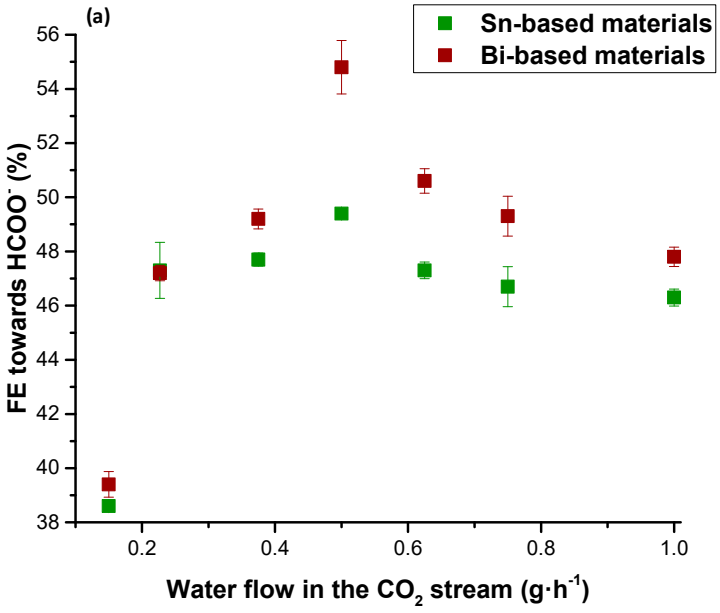

Figure 4. *Cont.*

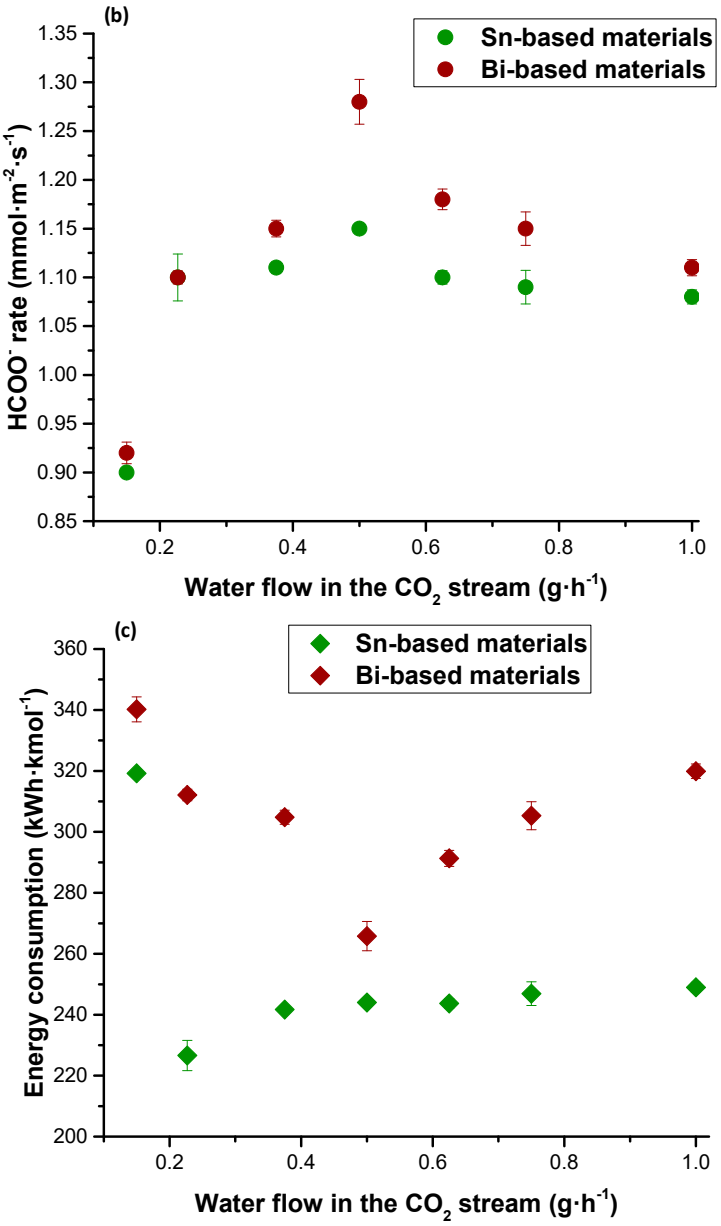

Figure 4. *Cont.*

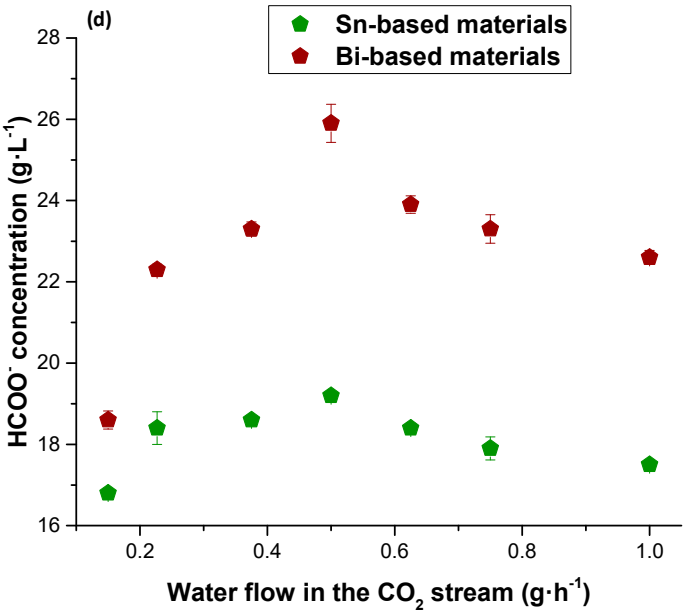

Figure 4. Influence of water flow in the CO_2 stream on (**a**) Faradaic efficiency for $HCOO^-$ (%), (**b**) $HCOO^-$ rate (mmol·m^{-2}·s–^{1}), (**c**) energy consumption per kmol of $HCOO^-$ (kWh·$kmol^{-1}$), and (**d**) $HCOO^-$ concentration (g·L^{-1}) in the water flow range of 0.15–1 g·h^{-1} applied at a constant current density = 45 mA·cm^{-2}, a catalyst loading = 0.75 mg·cm^{-2}, and a temperature = 20 °C Sn/C-CCMEs and Bi/C-CCMEs are indicated in green and red, respectively. Data taken from references [67,69].

4. Experimental Conditions

All the experiments considered in this comparative analysis were carried out working in a continuous mode with a single pass of the input streams through the electrochemical filter press reactor. The experimental setup included an electrochemical filter press reactor as the core element, a potentiostat–galvanostat, tanks, peristaltic pumps, and a Vapor Delivery Module for operating in a gaseous phase at the cathode side under the CCME configuration. In order to carry out a rigorous comparative study of the electrode configurations, the same electrocatalysts for both configurations were employed: (i) Sn/C-NPs or (ii) Bi/C-NPs. More detail about the synthesis and the characterization of Sn/C NPs and Bi/C-NPs are described in detail in Castillo et al. 2017 [66] and Ávila-Bolívar et al. 2019 [76], respectively.

In contrast, the behavior of the two different electrocatalysts (Sn/C NPs and Bi/C NPs) was compared under the same configuration and experimental setup in both studies: (i) GDEs (Figure 5a), which are described as detailed in Castillo et al. 2017 [66] and Díaz-Sainz et al. 2019 [68], and (ii) CCMEs (Figure 5b), whose fabrication and characterization are described in Díaz-Sainz et al. 2018 [67] and Díaz-Sainz et al. 2020 [69]. In this context, the size of both quasi-spherical Sn/C and Bi/C NPs are 10–15 nm and 9.3 ± 1.6 nm, respectively. The thickness values of the different layers shown in Figure 5 in each of the electrodes compared in this work are summarized in Table 4. In addition, the same operating conditions were employed in the references previously mentioned, as reviewed in Table 5.

In the GDE configuration, the current density and the liquid electrolyte flow per geometric area are considered key variables in the electrochemical conversion of CO_2 to $HCOO^-$, while in the CCMEs configuration, the key variables studied will be the temperature and the water flow in the input CO_2 stream. It is important to note that in the CCME configuration, due to the characteristics of CCME and unlike in GDEs, it is not feasible to work at high values of current density because this implies huge increases in cell potentials. This is why the comparison in Section 3.2. will be carried out using data at a fixed current density of 45 mA·cm^{-2}. In contrast, the temperature is only considered as a key variable for CCMEs because its influence in a GDE configuration is much more limited, but operating in a CCME configuration for the gas-phase electrocatalytic reduction of CO_2 to $HCOO^-$, this variable

has an important influence in the amount of water vapor condensed over the CCME surface as well as the water flow in the CO_2 input stream, which is a crucial aspect in the performance of the process.

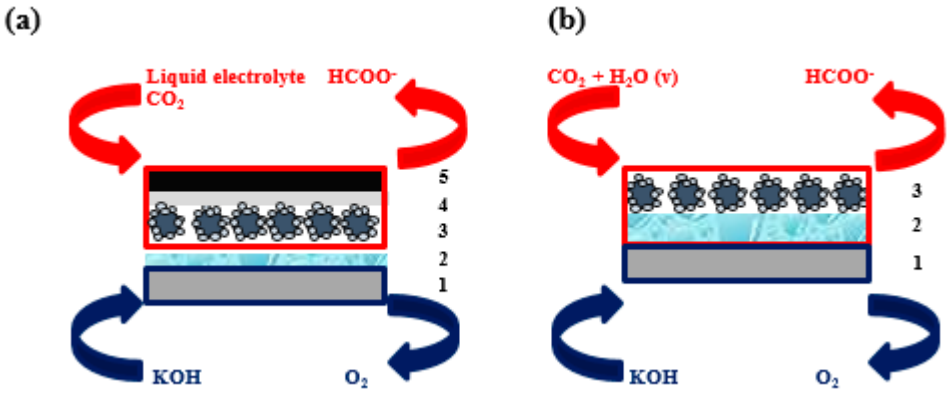

Figure 5. Scheme of (**a**) Gas Diffusion Electrode (GDE) configuration and (**b**) Catalyst Coated Membrane Electrode (CCME) configuration (1: the counter electrode; 2: the cationic exchange membrane; 3: the catalytic layer; 4: the microporous layer, and 5: the carbon support). Please note that there are no elements 4 and 5 in (**b**) because in the CCME configuration, the catalyst is deposited directly on the membrane, avoiding the use of a carbon support and microporous layer.

Table 4. Value of thickness of the different layers shown in Figure 5 in each of the electrodes employed in the references [66–69].

		Sn/C GDEs	Bi/C GDEs	Sn/C CCMEs	Bi/C CCMEs
Thickness	1	2 mm			
	2	183 µm			
	3	50–60 µm	15–20 µm	15 µm	15–20 µm
	4	100 µm	100–125 µm	No microporous layer	
	5	190 µm		No carbon support	

Finally, a Dimensionally Stable Anode (DSA) (number 1, Figure 5), a leak-free Ag/AgCl, and a Nafion 117 membrane (number 2, Figure 5) were used as a counter electrode, as a reference electrode, and as a cationic exchange membrane. In addition, the concentration of the $HCOO^-$ produced by the electrocatalytic reduction of CO_2 was analyzed by ion-chromatography technique.

Table 5. Value of the different operating conditions taken in the references [66–69].

Operating Condition	Value
Anolyte flow ($mL \cdot min^{-1}$)	5.7
KOH concentration in anolyte ($mol \cdot L^{-1}$)	1
CO_2 flow ($mL \cdot min^{-1}$)	200
Catalyst loading ($mg \cdot cm^{-2}$)	0.75
Reaction time (min)	90
Electrode area (cm^2)	10

5. Conclusions

This work is a comprehensive comparative assessment of different experimental data previously published after many years of research for the electrocatalytic reduction of CO_2 to $HCOO^-$ in different

working electrode configurations and electrocatalysts in a continuous mode with a single pass of the inputs through the reactor.

First, the comparison focused on operation with the same electrocatalyst: Sn/C NPs and Bi/C NPs, which were compared in different kinds of working electrode configurations. Considering the same electrocatalyst, the use of CCMEs improves the performance in terms of $HCOO^-$ concentration, Faradaic efficiency, and energy consumption when compared with GDEs of that same electrocatalyst. However, the $HCOO^-$ rate worsened because of the low values of current densities that had to be supplied to the electrochemical reactor in the CCME configuration.

Moreover, considering the same operating conditions, a rigorous comparison of both electrocatalysts in the form of GDEs and CCMEs has been carried out. Firstly, using Bi/C-GDEs, the performance of the electrochemical reactor was improved in all the figures of merit analyzed (FE for $HCOO^-$, $HCOO^-$ rate, energy consumption per kmol of $HCOO^-$, and $HCOO^-$ concentration) with respect to the Sn/C-GDEs operating at the same conditions. The same comparative study was performed using CCMEs as a cathode configuration. In this new scenario, the use of Bi/C NPs improved the $HCOO^-$ concentration in 35%, the FE for $HCOO^-$ in 11%, and the $HCOO^-$ rate in 11% with respect to the employ of Sn carbon-supported nanoparticles. Nevertheless, the energy consumption per kmol of $HCOO^-$ worsened with the use of Bi-based electrodes in 9%.

Finally, despite notable advances achieved, before the electrochemical conversion of CO_2 to $HCOO^-$ could be an industrial reality, further research is still required to optimize all the figures of merit analyzed in this study.

Author Contributions: Conceptualization, M.A.-G. and A.I.; Methodology, G.D.-S. and M.A.-G.; Investigation, G.D.-S.; Data Curation, G.D.-S. and M.A.-G.; Writing—Original Draft Preparation, G.D.-S. and M.A.-G.; Writing—Review and Editing, G.D.-S., M.A.-G. and A.I.; Visualization, G.D.-S. and M.A.-G.; Supervision, M.A.-G. and A.I.; Project Administration, A.I.; Funding Acquisition, A.I. All authors have read and agreed to the published version of the manuscript.

Funding: The authors of this work want to acknowledge financial support from the Spanish Ministry of Economy and Competitiveness, through the project CTQ2016-76231-C2-1-R (AEI/FEDER, UE).

Acknowledgments: The authors gratefully acknowledge the Spanish Ministry of Economy and Competitiveness, through the project CTQ2016-76231-C2-1-R (AEI/FEDER, UE) for financial support.

Conflicts of Interest: The authors declare no conflict of interest.

References

1. Overview of Greenhouse Gases: United States Environmental Protection Agency. Available online: https://www.epa.gov/ghgemissions/overview-greenhouse-gases (accessed on 16 June 2020).
2. Sustainable Development Goals: United Nations. Available online: https://sustainabledevelopment.un.org/ (accessed on 16 June 2020).
3. Irabien, A.; Alvarez-Guerra, M.; Albo, J.; Domínguez-Ramos, A. Electrochemical conversion of CO_2 to value-added products. In *Electrochememical Water Wastewater Treatment*; Martínez-Huitle, C.A., Rodrigo, M.A., Scialdone, O., Eds.; Elsevier: Amsterdam, The Netherlands, 2018; pp. 29–59.
4. Qiao, J.; Liu, Y.; Zhan, J. *Electrochemical Reduction of Carbon Dioxide. Fundamentals and Technologies*; CRC Press: Boca Raton, FL, USA, 2016; ISBN 9781482258257.
5. Bui, M.; Adjiman, C.S.; Bardow, A.; Anthony, E.J.; Boston, A.; Brown, S.; Fennell, P.S.; Fuss, S.; Galindo, A.; Hackett, L.A.; et al. Carbon capture and storage (CCS): The way forward. *Energy Environ. Sci.* **2018**, *11*, 1062–1176. [CrossRef]
6. Sohaib, Q.; Vadillo, J.M.; Gómez-Coma, L.; Albo, J.; Druon-Bocquet, S.; Irabien, A.; Sanchez-Marcano, J. CO_2 capture with room temperature ionic liquids; coupled absorption/desorption and single module absorption in membrane contactor. *Chem. Eng. Sci.* **2020**, *223*, 115719. [CrossRef]
7. Nocito, F.; Dibenedetto, A. Atmospheric CO_2 mitigation technologies: Carbon capture utilization and storage. *Curr. Opin. Green Sustain. Chem.* **2020**, *21*, 34–43. [CrossRef]
8. Mustafa, A.; Lougou, B.G.; Shuai, Y.; Wang, Z.; Tan, H. Current technology development for CO_2 utilization into solar fuels and chemicals: A review. *J. Energy Chem.* **2020**, *49*, 96–123. [CrossRef]

9. Vadillo, J.M.; Gómez-Coma, L.; Garea, A.; Irabien, A. CO_2 desorption performance from imidazolium ionic liquids by membrane vacuum regeneration technology. *Membranes* **2020**, *10*, 234. [CrossRef]
10. Lee, C.W.; Kim, C.; Min, B.K. Theoretical insights into selective electrochemical conversion of carbon dioxide. *Nano Converg.* **2019**, *6*, 8. [CrossRef]
11. Ting, L.R.L.; Yeo, B.S. Recent advances in understanding mechanisms for the electrochemical reduction of carbon dioxide. *Curr. Opin. Electrochem.* **2018**, *8*, 126–134. [CrossRef]
12. Zheng, Y.; Zhang, W.; Li, Y.; Chen, J.; Yu, B.; Wang, J.; Zhang, L.; Zhang, J. Energy related CO_2 conversion and utilization: Advanced materials/nanomaterials, reaction mechanisms and technologies. *Nano Energy* **2017**, *40*, 512–539. [CrossRef]
13. Yaashikaa, P.R.; Senthil Kumar, P.; Varjani, S.J.; Saravanan, A. A review on photochemical, biochemical and electrochemical transformation of CO_2 into value-added products. *J. CO_2 Util.* **2019**, *33*, 131–147. [CrossRef]
14. Merino-Garcia, I.; Alvarez-Guerra, E.; Albo, J.; Irabien, A. Electrochemical membrane reactors for the utilisation of carbon dioxide. *Chem. Eng. J.* **2016**, *305*, 104–120. [CrossRef]
15. Castro, S.; Albo, J.; Irabien, A. Photoelectrochemical Reactors for CO_2 Utilization. *ACS Sustain. Chem. Eng.* **2018**, *6*, 15877–15894. [CrossRef]
16. Kumar, B.; Brian, J.P.; Atla, V.; Kumari, S.; Bertram, K.A.; White, R.T.; Spurgeon, J.M. New trends in the development of heterogeneous catalysts for electrochemical CO_2 reduction. *Catal. Today* **2016**, *270*, 19–30. [CrossRef]
17. Lu, Q.; Jiao, F. Electrochemical CO_2 reduction: Electrocatalyst, reaction mechanism, and process engineering. *Nano Energy* **2016**, *29*, 439–456. [CrossRef]
18. Endrődi, B.; Bencsik, G.; Darvas, F.; Jones, R.; Rajeshwar, K.; Janáky, C. Continuous-flow electroreduction of carbon dioxide. *Prog. Energy Combust. Sci.* **2017**, *62*, 133–154. [CrossRef]
19. Gao, D.; Arán-Ais, R.M.; Jeon, H.S.; Roldan Cuenya, B. Rational catalyst and electrolyte design for CO_2 electroreduction towards multicarbon products. *Nat. Catal.* **2019**, *2*, 198–210. [CrossRef]
20. Ren, S.; Joulié, D.; Salvatore, D.; Torbensen, K.; Wang, M.; Robert, M.; Berlinguette, C.P. Molecular electrocatalysts can mediate fast, selective CO_2 reduction in a flow cell. *Science* **2019**, *365*, 367–369. [CrossRef]
21. Jouny, M.; Hutchings, G.S.; Jiao, F. Carbon monoxide electroreduction as an emerging platform for carbon utilization. *Nat. Catal.* **2019**, *2*, 1062–1070. [CrossRef]
22. Du, D.; Lan, R.; Humphreys, J.; Tao, S. Progress in inorganic cathode catalysts for electrochemical conversion of carbon dioxide into formate or formic acid. *J. Appl. Electrochem.* **2017**, *47*, 661–678. [CrossRef]
23. Taheri, A.; Berben, L.A. Making C-H bonds with CO_2: Production of formate by molecular electrocatalysts. *Chem. Commun.* **2016**, *52*, 1768–1777. [CrossRef]
24. Wu, Y.; Jiang, Z.; Lu, X.; Liang, Y.; Wang, H. Domino electroreduction of CO_2 to methanol on a molecular catalyst. *Nature* **2019**, *575*, 639–642. [CrossRef]
25. Nitopi, S.; Bertheussen, E.; Scott, S.B.; Liu, X.; Engstfeld, A.K.; Horch, S.; Seger, B.; Stephens, I.E.L.; Chan, K.; Hahn, C.; et al. Progress and Perspectives of Electrochemical CO_2 Reduction on Copper in Aqueous Electrolyte. *Chem. Rev.* **2019**, *119*, 7610–7672. [CrossRef] [PubMed]
26. Zhang, W.; Hu, Y.; Ma, L.; Zhu, G.; Wang, Y.; Xue, X.; Chen, R.; Yang, S.; Jin, Z. Progress and Perspective of Electrocatalytic CO_2 Reduction for Renewable Carbonaceous Fuels and Chemicals. *Adv. Sci.* **2018**, *5*, 1700275. [CrossRef] [PubMed]
27. Zhang, L.; Merino-Garcia, I.; Albo, J.; Sánchez-Sánchez, C.M. Electrochemical CO_2 reduction reaction on cost-effective oxide-derived copper and transition metal–nitrogen–carbon catalysts. *Curr. Opin. Electrochem.* **2020**, *23*, 65–73. [CrossRef]
28. Zhao, J.; Xue, S.; Barber, J.; Zhou, Y.; Meng, J.; Ke, X. An overview of Cu-based heterogeneous electrocatalysts for CO_2 reduction. *J. Mater. Chem. A* **2020**, *8*, 4700–4734. [CrossRef]
29. Agarwal, A.S.; Zhai, Y.; Hill, D.; Sridhar, N. The electrochemical reduction of carbon dioxide to formate/formic acid: Engineering and economic feasibility. *ChemSusChem* **2011**, *4*, 1301–1310. [CrossRef]
30. Bienen, F.; Kopljar, D.; Löwe, A.; Aßmann, P.; Stoll, M.; Rößner, P.; Wagner, N.; Friedrich, A.; Klemm, E. Utilizing Formate as an Energy Carrier by Coupling CO_2 Electrolysis with Fuel Cell Devices. *Chem. Ing. Tech.* **2019**, *91*, 872–882. [CrossRef]
31. An, L.; Chen, R. Direct formate fuel cells: A review. *J. Power Sources* **2016**, *320*, 127–139. [CrossRef]
32. Preuster, P.; Albert, J. Biogenic Formic Acid as a Green Hydrogen Carrier. *Energy Technol.* **2018**, *6*, 501–509. [CrossRef]

33. Eppinger, J.; Huang, K.W. Formic Acid as a Hydrogen Energy Carrier. *ACS Energy Lett.* **2017**, *2*, 188–195. [CrossRef]
34. Han, N.; Ding, P.; He, L.; Li, Y.; Li, Y. Promises of Main Group Metal–Based Nanostructured Materials for Electrochemical CO_2 Reduction to Formate. *Adv. Energy Mater.* **2019**, *10*, 1902338. [CrossRef]
35. Zhao, S.; Li, S.; Guo, T.; Zhang, S.; Wang, J.; Wu, Y.; Chen, Y. Advances in Sn-Based Catalysts for Electrochemical CO_2 Reduction. *Nano-Micro Lett.* **2019**, *11*, 62. [CrossRef]
36. Sen, S.; Liu, D.; Palmore, G.T.R. Electrochemical reduction of CO_2 at copper nanofoams. *ACS Catal.* **2014**, *4*, 3091–3095. [CrossRef]
37. Gao, S.; Lin, Y.; Jiao, X.; Sun, Y.; Luo, Q.; Zhang, W.; Li, D.; Yang, J.; Xie, Y. Partially oxidized atomic cobalt layers for carbon dioxide electroreduction to liquid fuel. *Nature* **2016**, *529*, 68–71. [CrossRef] [PubMed]
38. Yuan, M.; Sahin, S.; Cai, R.; Abdellaoui, S.; Hickey, D.P.; Minteer, S.D.; Milton, R.D. Creating a Low-Potential Redox Polymer for Efficient Electroenzymatic CO_2 Reduction. *Angew. Chem. Int. Ed.* **2018**, *57*, 6582–6586. [CrossRef] [PubMed]
39. Pander, J.E.; Lum, J.W.J.; Yeo, B.S. The importance of morphology on the activity of lead cathodes for the reduction of carbon dioxide to formate. *J. Mater. Chem. A* **2019**, *7*, 4093–4101. [CrossRef]
40. Alvarez-Guerra, M.; Quintanilla, S.; Irabien, A. Conversion of carbon dioxide into formate using a continuous electrochemical reduction process in a lead cathode. *Chem. Eng. J.* **2012**, *207–208*, 278–284. [CrossRef]
41. Gálvez-Vázquez, M.D.J.; Moreno-García, P.; Guo, H.; Hou, Y.; Dutta, A.; Waldvogel, S.R.; Broekmann, P. Leaded Bronze Alloy as a Catalyst for the Electroreduction of CO_2. *ChemElectroChem* **2019**, *6*, 2324–2330. [CrossRef]
42. Luo, W.; Xie, W.; Li, M.; Zhang, J.; Züttel, A. 3D hierarchical porous indium catalyst for highly efficient electroreduction of CO_2. *J. Mater. Chem. A* **2019**, *7*, 4505–4515. [CrossRef]
43. Zha, B.; Li, C.; Li, J. Efficient electrochemical reduction of CO_2 into formate and acetate in polyoxometalate catholyte with indium catalyst. *J. Catal.* **2020**, *382*, 69–76. [CrossRef]
44. Yuan, X.; Luo, Y.; Zhang, B.; Dong, C.; Lei, J.; Yi, F.; Duan, T.; Zhu, W.; He, R. Decoration of in nanoparticles on In2S3 nanosheets enables efficient electrochemical reduction of CO_2. *Chem. Commun.* **2020**, *56*, 4212–4215. [CrossRef]
45. Klinkova, A.; De Luna, P.; Dinh, C.T.; Voznyy, O.; Larin, E.M.; Kumacheva, E.; Sargent, E.H. Rational Design of Efficient Palladium Catalysts for Electroreduction of Carbon Dioxide to Formate. *ACS Catal.* **2016**, *6*, 8115–8120. [CrossRef]
46. Gao, D.; Zhou, H.; Cai, F.; Wang, D.; Hu, Y.; Jiang, B.; Cai, W.-B.; Chen, X.; Si, R.; Yang, F.; et al. Switchable CO_2 electroreduction via engineering active phases of Pd nanoparticles. *Nano Res.* **2017**, *10*, 2181–2191. [CrossRef]
47. Lee, W.; Kim, Y.E.; Youn, M.H.; Jeong, S.K.; Park, K.T. Catholyte-Free Electrocatalytic CO_2 Reduction to Formate. *Angew. Chem. Int. Ed.* **2018**, *57*, 6883–6887. [CrossRef]
48. Li, D.; Wu, J.; Liu, T.; Liu, J.; Yan, Z.; Zhen, L.; Feng, Y. Tuning the pore structure of porous tin foam electrodes for enhanced electrochemical reduction of carbon dioxide to formate. *Chem. Eng. J.* **2019**, *375*, 122024. [CrossRef]
49. He, G.; Tang, H.; Wang, H.; Bian, Z. Highly Selective and Active Pd-In/three-dimensional Graphene with Special Structure for Electroreduction CO_2 to Formate. *Electroanalysis* **2018**, *30*, 84–93. [CrossRef]
50. Proietto, F.; Schiavo, B.; Galia, A.; Scialdone, O. Electrochemical conversion of CO_2 to HCOOH at tin cathode in a pressurized undivided filter-press cell. *Electrochim. Acta* **2018**, *277*, 30–40. [CrossRef]
51. Alvarez-Guerra, M.; Del Castillo, A.; Irabien, A. Continuous electrochemical reduction of carbon dioxide into formate using a tin cathode: Comparison with lead cathode. *Chem. Eng. Res. Des.* **2014**, *92*, 692–701. [CrossRef]
52. Del Castillo, A.; Alvarez-Guerra, M.; Irabien, A. Continuous electroreduction of CO_2 to formate using Sn gas diffusion electrodes. *AIChE J.* **2014**, *60*, 3557–3564. [CrossRef]
53. Del Castillo, A.; Alvarez-Guerra, M.; Solla-Gullón, J.; Sáez, A.; Montiel, V.; Irabien, A. Electrocatalytic reduction of CO_2 to formate using particulate Sn electrodes: Effect of metal loading and particle size. *Appl. Energy* **2015**, *157*, 165–173. [CrossRef]

54. Fu, Y.; Wang, T.; Zheng, W.; Lei, C.; Yang, B.; Chen, J.; Li, Z.; Lei, L.; Yuan, C.; Hou, Y. Nanoconfined Tin Oxide within N-Doped Nanocarbon Supported on Electrochemically Exfoliated Graphene for Efficient Electroreduction of CO_2 to Formate and C1 Products. *ACS Appl. Mater. Interf.* **2020**, *12*, 16178–16185. [CrossRef]
55. Zhang, X.; Sun, X.; Guo, S.-X.; Bond, A.M.; Zhang, J. Formation of lattice-dislocated bismuth nanowires on copper foam for enhanced electrocatalytic CO_2 reduction at low overpotential. *Energy Environ. Sci.* **2019**, *12*, 1334–1340. [CrossRef]
56. Wu, D.; Huo, G.; Chen, W.Y.; Fu, X.Z.; Luo, J.L. Boosting formate production at high current density from CO_2 electroreduction on defect-rich hierarchical mesoporous Bi/Bi_2O_3 junction nanosheets. *Appl. Catal. B Environ.* **2020**, *271*, 118957. [CrossRef]
57. Wang, Q.; Zhu, C.; Wu, C.; Yu, H. Direct synthesis of bismuth nanosheets on a gas diffusion layer as a high-performance cathode for a coupled electrochemical system capable of electroreduction of CO_2 to formate with simultaneous degradation of organic pollutants. *Electrochim. Acta* **2019**, *319*, 138–147. [CrossRef]
58. Yang, F.; Elnabawy, A.O.; Schimmenti, R.; Song, P.; Wang, J.; Peng, Z.; Yao, S.; Deng, R.; Song, S.; Lin, Y.; et al. Bismuthene for highly efficient carbon dioxide electroreduction reaction. *Nat. Commun.* **2020**, *11*, 1088. [CrossRef] [PubMed]
59. Zhu, C.; Wang, Q.; Wu, C. Rapid and scalable synthesis of bismuth dendrites on copper mesh as a high-performance cathode for electroreduction of CO_2 to formate. *J. CO_2 Util.* **2020**, *36*, 96–104. [CrossRef]
60. Tran-Phu, T.; Daiyan, R.; Fusco, Z.; Ma, Z.; Amal, R.; Tricoli, A. Nanostructured β-Bi2O3 Fractals on Carbon Fibers for Highly Selective CO_2 Electroreduction to Formate. *Adv. Funct. Mater.* **2020**, *30*, 1–8. [CrossRef]
61. Lu, P.; Gao, D.; He, H.; Wang, Q.; Liu, Z.; Dipazir, S.; Yuan, M.; Zu, W.; Zhang, G. Facile synthesis of a bismuth nanostructure with enhanced selectivity for electrochemical conversion of CO_2 to formate. *Nanoscale* **2019**, *11*, 7805–7812. [CrossRef]
62. García de Arquer, F.P.; Bushuyev, O.S.; De Luna, P.; Dinh, C.T.; Seifitokaldani, A.; Saidaminov, M.I.; Tan, C.S.; Quan, L.N.; Proppe, A.; Kibria, M.G.; et al. 2D Metal Oxyhalide-Derived Catalysts for Efficient CO_2 Electroreduction. *Adv. Mater.* **2018**, *30*, 6–11. [CrossRef]
63. Kumawat, A.S.; Sarkar, A. Comparative Study of Carbon Supported Pb, Bi and Sn Catalysts for Electroreduction of Carbon Dioxide in Alkaline Medium. *J. Electrochem. Soc.* **2017**, *164*, H1112–H1120. [CrossRef]
64. Vennekoetter, J.B.; Sengpiel, R.; Wessling, M. Beyond the catalyst: How electrode and reactor design determine the product spectrum during electrochemical CO_2 reduction. *Chem. Eng. J.* **2019**, *364*, 89–101. [CrossRef]
65. Vennekötter, J.B.; Scheuermann, T.; Sengpiel, R.; Wessling, M. The electrolyte matters: Stable systems for high rate electrochemical CO_2 reduction. *J. CO_2 Util.* **2019**, *32*, 202–213.
66. Del Castillo, A.; Alvarez-Guerra, M.; Solla-Gullón, J.; Sáez, A.; Montiel, V.; Irabien, A. Sn nanoparticles on gas diffusion electrodes: Synthesis, characterization and use for continuous CO_2 electroreduction to formate. *J. CO_2 Util.* **2017**, *18*, 222–228. [CrossRef]
67. Díaz-Sainz, G.; Alvarez-Guerra, M.; Solla-Gullón, J.; García-Cruz, L.; Montiel, V.; Irabien, A. Catalyst coated membrane electrodes for the gas phase CO_2 electroreduction to formate. *Catal. Today* **2020**, *346*, 58–64. [CrossRef]
68. Díaz-Sainz, G.; Alvarez-Guerra, M.; Solla-Gullón, J.; García-Cruz, L.; Montiel, V.; Irabien, A. CO_2 electroreduction to formate: Continuous single-pass operation in a filter-press reactor at high current densities using Bi gas diffusion electrodes. *J. CO_2 Util.* **2019**, *34*, 12–19.
69. Díaz-Sainz, G.; Alvarez-Guerra, M.; Solla-Gullón, J.; García-Cruz, L.; Montiel, V.; Irabien, A. Gas–liquid–solid reaction system for CO_2 electroreduction to formate without using supporting electrolyte. *AIChE J.* **2020**, *66*, e16299.
70. Xia, C.; Zhu, P.; Jiang, Q.; Pan, Y.; Liang, W.; Stavitsk, E. Continuous production of pure liquid fuel solutions via electrocatalytic CO_2 reduction using solid-electrolyte devices. *Nat. Energy* **2019**, *5*, 776–785. [CrossRef]
71. Díaz-Sainz, G.; Alvarez-Guerra, M.; Ávila-Bolívar, B.; Solla-Gullón, J.; Montiel, V.; Irabien, A. Improving trade-offs in the figures of merit of gas-phase single-pass continuous CO_2 electrocatalytic reduction to formate. *Chem. Eng. J.* **2020**, *405*, 126965. [CrossRef]

72. Chen, Y.; Vise, A.; Klein, W.E.; Cetinbas, F.C.; Myers, D.J.; Smith, W.A.; Deutsch, T.G.; Neyerlin, K.C. A Robust, Scalable Platform for the Electrochemical Conversion of CO_2 to Formate: Identifying Pathways to Higher Energy Efficiencies. *ACS Energy Lett.* **2020**, *5*, 1825–1833. [CrossRef]
73. Marcos-Madrazo, A.; Casado-Coterillo, C.; Irabien, Á. Sustainable Membrane-Coated Electrodes for CO_2 Electroreduction to Methanol in Alkaline Media. *ChemElectroChem* **2019**, *6*, 5273–5282. [CrossRef]
74. Merino-Garcia, I.; Albo, J.; Krzywda, P.; Mul, G.; Irabien, A. Bimetallic Cu-based hollow fibre electrodes for CO_2 electroreduction. *Catal. Today* **2020**, *346*, 34–39. [CrossRef]
75. Hosseini, M.G.; Mahmoodi, R.; Daneshvari-Esfahlan, V. Ni@Pd core-shell nanostructure supported on multi-walled carbon nanotubes as efficient anode nanocatalysts for direct methanol fuel cells with membrane electrode assembly prepared by catalyst coated membrane method. *Energy* **2018**, *161*, 1074–1084. [CrossRef]
76. Ávila-Bolívar, B.; García-Cruz, L.; Montiel, V.; Solla-Gullón, J. Electrochemical Reduction of CO_2 to Formate on Easily Prepared Carbon-Supported Bi Nanoparticles. *Molecules* **2019**, *24*, 2032.